Korea-Australia Rheology Journal, 30(3), 161-167 (August 2018) www.springer.com/13367
DOI: 10.1007/s13367-018-0016-8

Application of injection-compression molding to thin-walled polymeric parts

Young Il Kwon and Young Seok Song*
Department of Fiber System Engineering, Dankook University, Yongin 16890, Republic of Korea
(Received March 14, 2018; final revision received April 18, 2018; accepted April 27, 2018)

In this study, we investigated the injection molding (IM) process for the production polymeric parts with thin walls. The injection molding process was numerically modelled, and thin-walled polymeric parts were injection-molded experimentally. In the case of polymeric parts with thin walls, it is critical to understand flow and heat transfer behavior in the mold during the process. Injection-compression molding (ICM) was adopted to fabricate the parts, and the resulting residual stress and warpage were evaluated. In addition, birefringence of the molded part was analyzed to validate the numerical results.

Keywords: thin, injection, compression, molding

1. Introduction

Injection molding is a fascinating manufacturing process that has many strong points, such as low cost, good processability, high precision, and good surface finish (Guevara-Morales and Figueroa-López, 2014; Oh *et al.*, 2011). These days, the molding process is being used to fabricate from nano-sized through macro-sized parts in manifold applications, such as microelectronics, automobile, and automotive (Hong *et al.*, 2015; Oh and Song, 2015). In particular, much effort has been made to manufacture large areal, and thin polymeric parts, such as battery cases, light guide panels, and plastic window using injection molding (Min and Yoon, 2011). However, it still remains a challenge due to relatively fast heat transfer in the mold and low flowability of polymer melt (Chen *et al.*, 2013; Guevara-Morales and Figueroa-López, 2014; Isayev *et al.*, 2006). In the injection molding process, polymer is solidified and a skin layer is generated right after a polymer melt is injected into a mold cavity (Oh and Song, 2017). Basically, this acts as an inherent barrier to overcome for the enhancement of the low moldability (Jiang *et al.*, 2007; Kabanemi *et al.*, 1998; Kamal *et al.*, 2002). On the other hand, injection compression molding (ICM) combines injection molding with compression molding to produce large and thin polymeric components (Chen *et al.*, 1998). After the filling stage of injection molding, additional clamping force is applied to a mold, and the mold cavity is squeezed. Even though the ICM process can shorten the thickness of molded parts, significantly enhanced residual stress necessarily arises from the additional pressure. As a result, structural deformation of parts such as warpage and deflection is likely to occur (Ozcelik and Sonat, 2009).

Numerical modelling of injection molding allows us to understand the entire process in a more systematic manner (Teixeira *et al.*, 2015; Weng *et al.*, 2009a). For instance, results of flow simulation can help design a mold and determine flow velocity and pressure of injection molding to avoid incomplete cavity filling and weld lines (Weng *et al.*, 2009b). Heat transfer in the mold and solidification during filling and cooling can be simulated numerically. Based on the results, operational processing conditions such as cycle time, melt temperature, and mold wall temperature can be controlled. Furthermore, this enables us to design and manufacture optimal final products by manipulating post-processing properties such as residual stress and shrinkage.

In the current study, the ICM process was numerically simulated. Thin and large battery cases were designed and manufactured using the process. Flow behavior in the cavity was analyzed with respect to time, and the pressure and temperature distributions of parts were investigated. Then, the residual stress was evaluated and compared with the result of birefringence obtained experimentally.

2. Experimental

2.1. Sample preparation

Polycarbonate (PC) and acrylonitrile butadiene styrene (ABS) copolymer supplied by SABIC Corporation (CYCOLOYCX7240) were blended and used for the injection molding. Before the process, the polymeric pellets were fully dried by using a convection oven. Velocity/pressure switching was applied when 98% of the cavity volume was filled. The detailed processing conditions of injection molding are listed in Table 1.

2.2. Numerical analysis

In this study, we exploited the ICM for the preparation of thin battery cases. The ICM processes were numerically modelled using a commercial CFD software, Moldex3D. The conservation of mass, conservation of linear momentum, and conservation of energy were used as gov-

*Corresponding author; E-mail: ysong@dankook.ac.kr

Table 1. Processing conditions used in this study.

Filling time	0.3 s
Packing pressure	80 MPa
Cooling time	20 s
Melt temperature	285°C
Mold temperature	106°C
Ejection temperature	94°C

erning equations (Oh and Song, 2015):

$$\frac{d\rho}{dt} + \rho(\nabla \cdot \tilde{v}) = 0\,, \tag{1}$$

$$\rho\frac{d\tilde{v}}{dt} = -\nabla P + \nabla \cdot \tilde{\tau} + \rho\tilde{g}\,, \tag{2}$$

$$\rho C_p \frac{dT}{dt} = \beta T \frac{dP}{dt} + \eta\dot{\gamma}^2 + \nabla \cdot \tilde{q} \tag{3}$$

where ρ is the density, $\tilde{v}$ is the velocity vector, P is the pressure, $\tilde{\tau}$ is the viscous stress tensor, $\tilde{g}$ is the gravity vector, C_p is the specific heat at constant pressure, β is the thermal expansion coefficient, η is the generalized Newtonian viscosity, and $\tilde{q}$ is the heat flux vector. The magnitude of shear rate tensor, $\dot{\gamma}$ is simplified in the Cartesian coordinate system as below:

$$\dot{\gamma} = \sqrt{\left(\frac{\partial u}{\partial z}\right)^2 + \left(\frac{\partial v}{\partial z}\right)^2} \tag{4}$$

where (u, v) are the velocity components in the (x, y) directions. The accurate location of the melt flow front in the cavity was predicted using the following fluid concentration equation:

$$\frac{dF}{dt} = 0 \tag{5}$$

where F is the fluid concentration. The flow property of polymer melt was described with the 5 constant modified Cross model:

$$\eta(T, \dot{\gamma}, P) = \frac{\eta_0(T, P)}{1 + (\eta_0(T, P)\dot{\gamma}/\tau^*)^{1-n}} \tag{6}$$

where η is the viscosity, η_0 is the zero shear rate viscosity, τ^* is the shear stress at the transition between the Newtonian and the Power-law behaviors, and n is the Power-law index. η_0 can be represented as a function of temperature using the Williams-Landel-Ferry (WLF) equation:

$$\eta_0(T, P) = D_1 \exp\left(-\frac{A_1(T - T^*(P))}{A_2 + D_3P + (T - T^*(P))}\right) \tag{7}$$

where $T^*(P) = D_2 + D_3P$. The material constants for Eqs. (6) and (7) are taken from Moldex3D.

3. Results and Discussion

Figure 1 presents the melt front in the mold cavity with respect to time. The eight gates were used for the resin filling. It was found that the melt front filled the cavity progressively. The multi-gates were employed for manufacturing large and thin parts. Therefore, several weld lines were identified. Since the thickness of the part was 0.31 mm, relatively high filling pressure and short filling time were needed to avoid the so-called 'short-shot'. This is one of the main reasons to adopt ICM, *i.e.*, relatively low filling pressure.

Figure 2 shows the sprue pressure, flow rate, clamping force, volume fraction, and total weight for the cavity during filling in the process. As shown in Fig. 2a, the sprue pressure was first gradually increased over time until the runners were fully filled. After then, the sprue pressure was dramatically increased up to 98.52 MPa. Consequently, the flow rate was remarkably increased and then reversed (Fig. 2b). This was ascribed to the compression. The clamping force was also sharply increased and decreased as a function of time (Fig. 2c). Figure 2d demonstrates that a volume fraction of 73% of the cavity was filled in the resin injection stage and the remaining volume (*i.e.*, 37%) was done in the compression stage.

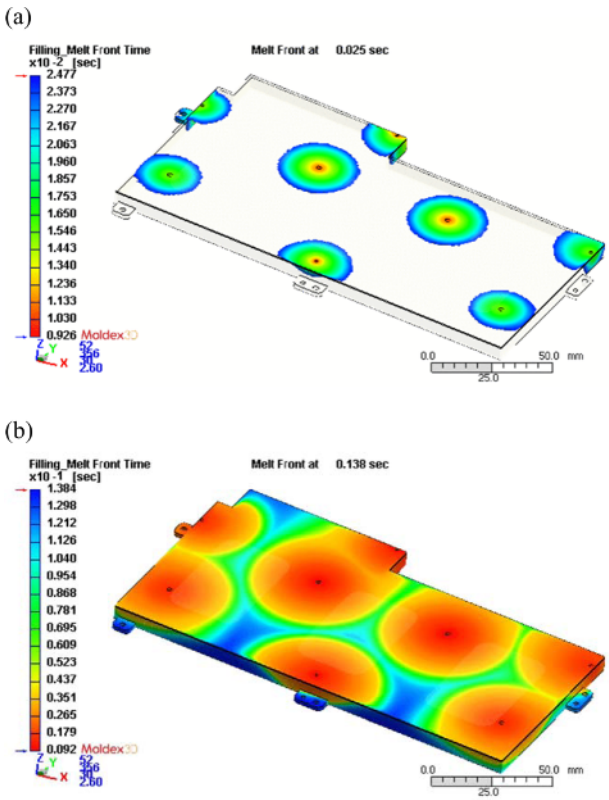

Fig. 1. (Color online) Melt front of polymer in the mold cavity with respect to time: (a) 0.025 s and (b) 0.138 s.

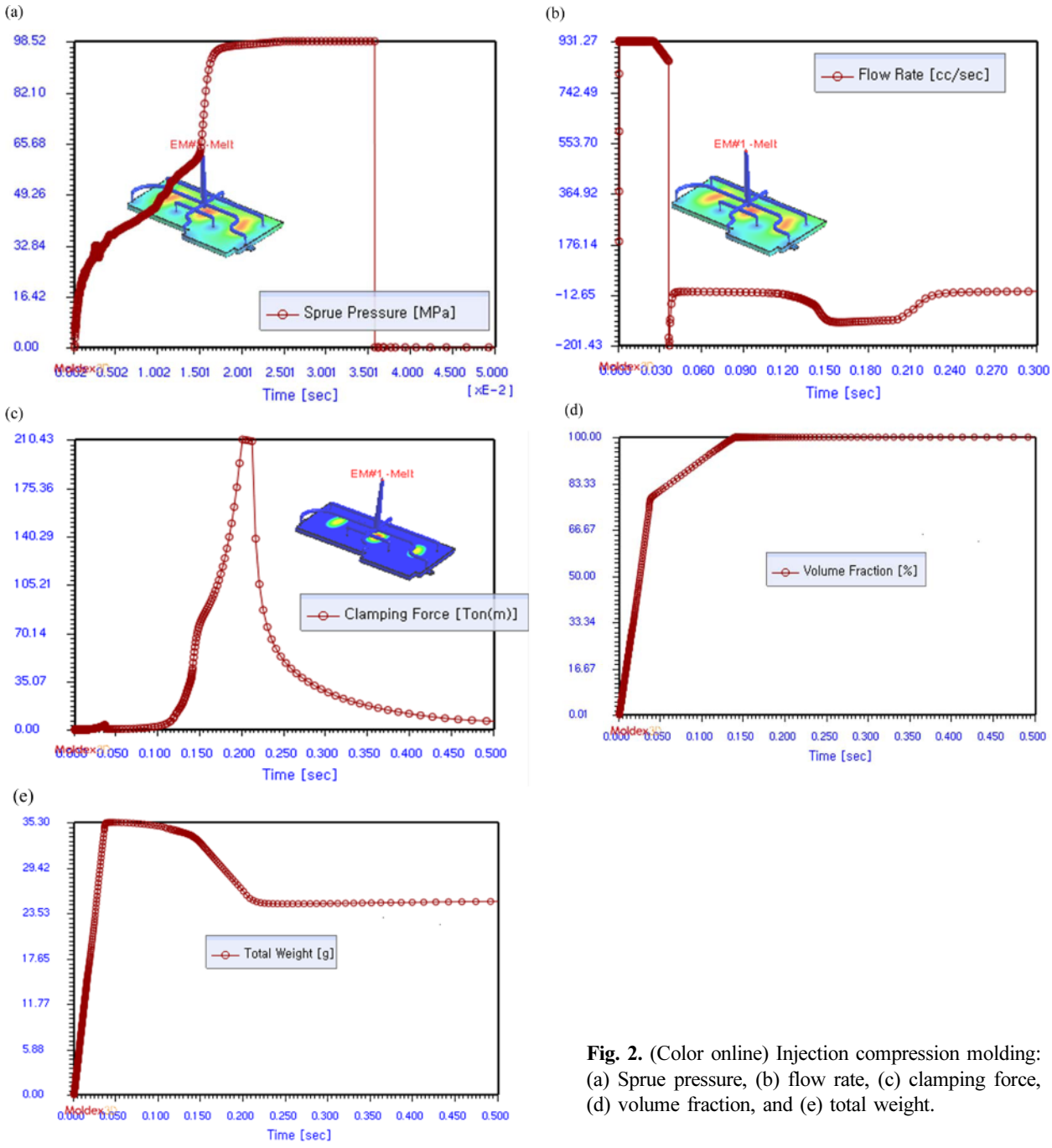

Fig. 2. (Color online) Injection compression molding: (a) Sprue pressure, (b) flow rate, (c) clamping force, (d) volume fraction, and (e) total weight.

The total weight changed over time, which was similar to the result of flow rate (Fig. 2e). In the injection molding, the fill time was set at 0.3 s. The pressure distribution during ICM is presented in Fig. 3. The sections with a relatively lower thickness (0.31 mm) was found to have higher pressure values. After the filling step (0.3 s), the pressure was dropped rapidly. The temperature distribution during ICM is displayed in Fig. 4. As expected, the sections with a lower thickness were cooled first and frozen.

Figure 5 shows the percentage of frozen layer during ICM. It turned out that the thinner part was frozen at 0.6 s first, and the entire part was followed at 10 s. The warpage of the molded part in the thickness direction is presented in Fig. 6. The numerically predicted warpage was found to be about 1.3 mm. In general, the residual stress of injection molded parts is explained with two mechanisms, *i.e.*, flow induced residual stress and thermal-induced residual stress. The former arises from the orientation of molecules by hydrodynamic stress, and the latter

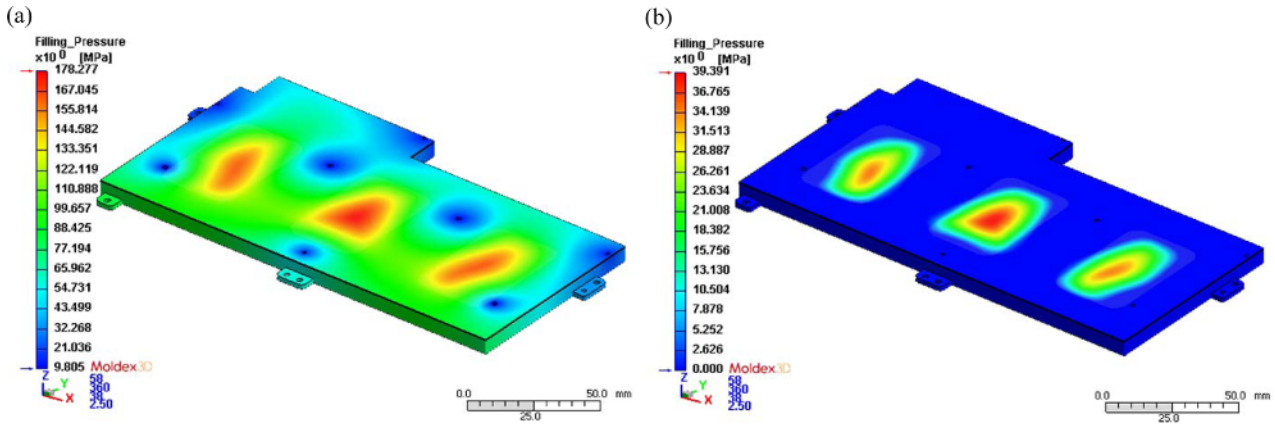

Fig. 3. (Color online) Pressure distribution during ICM: (a) 0.215 s and (b) 0.473 s.

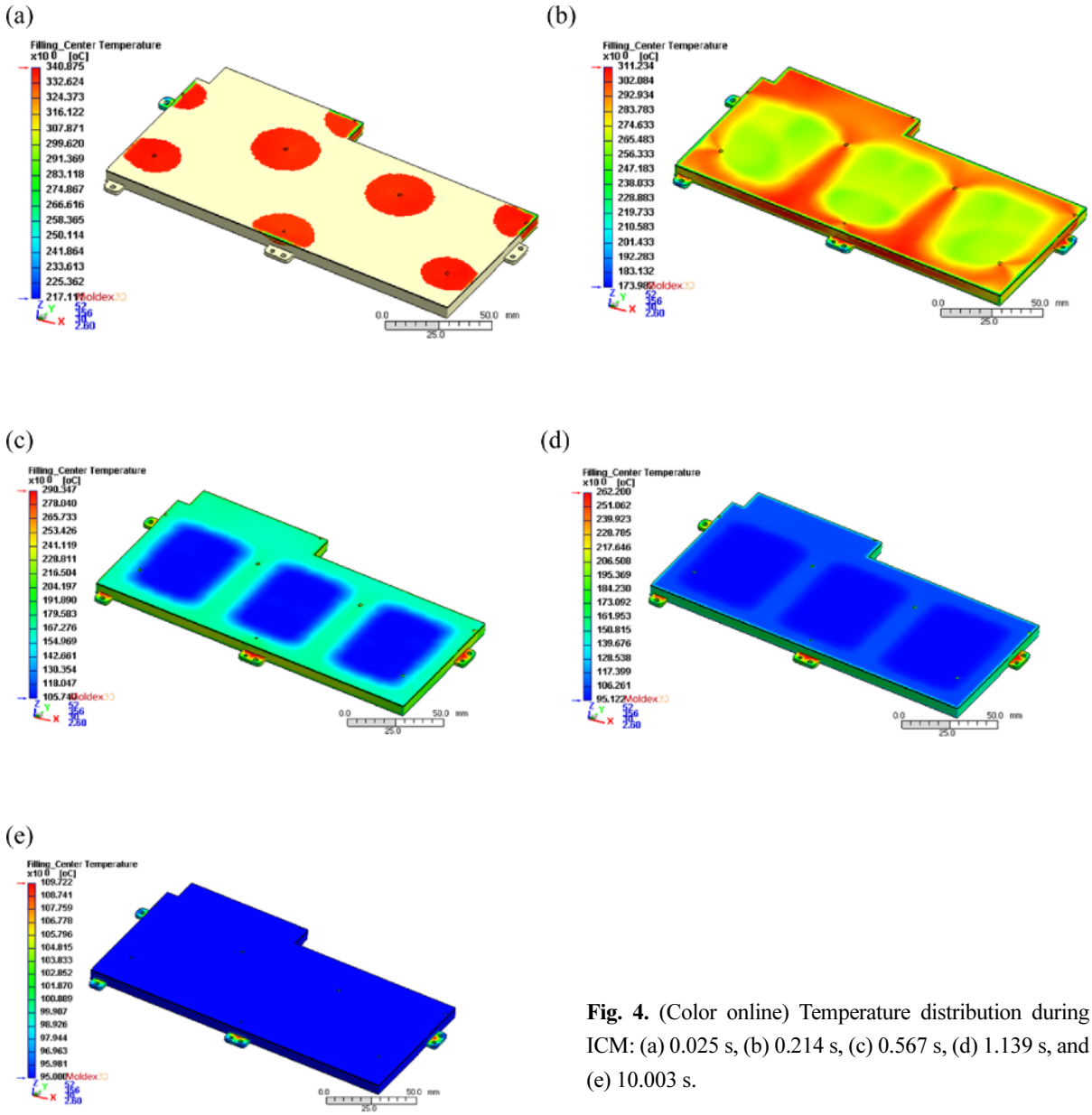

Fig. 4. (Color online) Temperature distribution during ICM: (a) 0.025 s, (b) 0.214 s, (c) 0.567 s, (d) 1.139 s, and (e) 10.003 s.

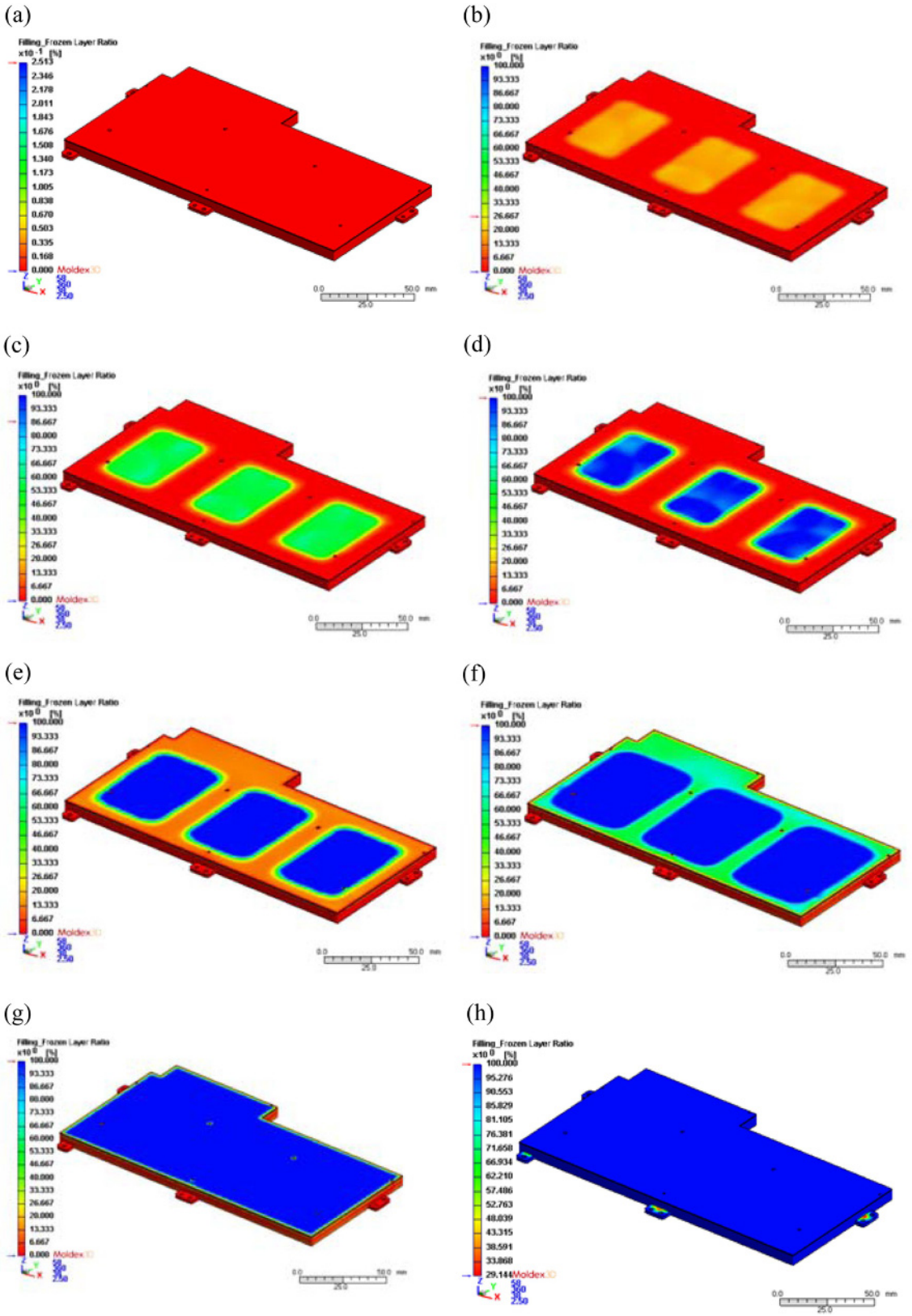

Fig. 5. (Color online) Percentage of frozen layer during ICM: (a) 0.215 s, (b) 0.473 s, (c) 0.548 s, (d) 0.569 s, (e) 0.813 s, (f) 1.092 s, (g) 1.191 s, and (h) 10.004 s.

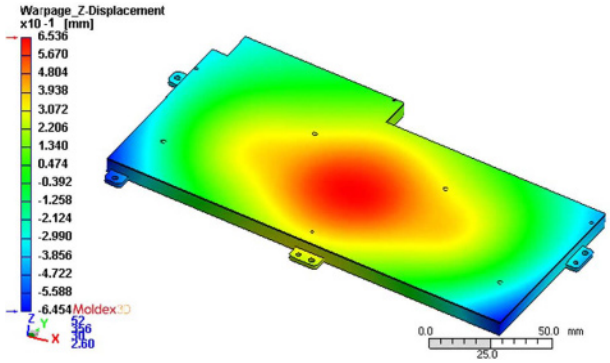

Fig. 6. (Color online) Warpage of the molded part in the thickness direction.

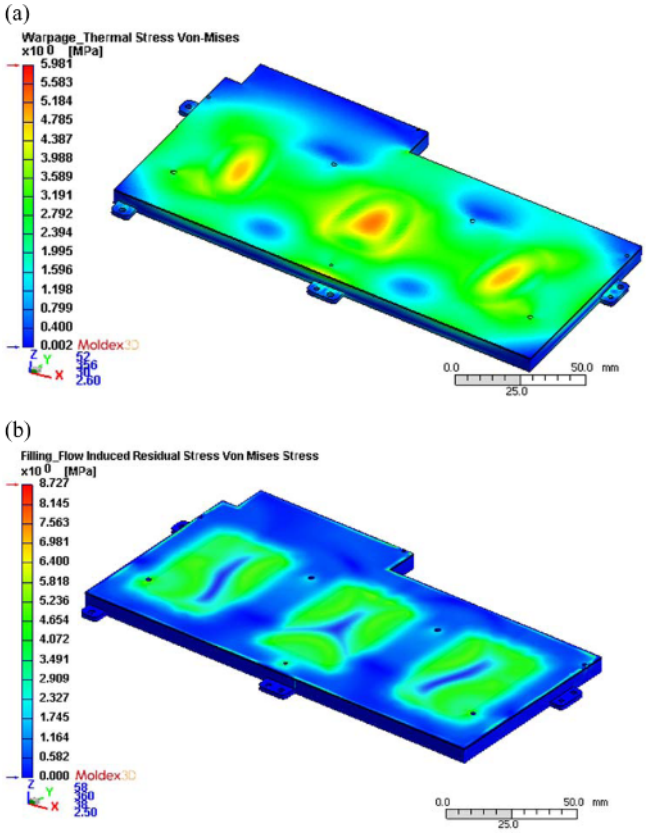

Fig. 7. (Color online) Residual stress of the molded part: (a) Thermal-induced residual stress and (b) flow-induced residual stress.

is due to the non-uniformity of temperature distribution during process. Figure 7 shows the residual stress distribution of the molded parts. The results revealed that the thermally induced residual stress was higher than the flow induced residual stress. These results were compared with the birefringence result as shown in Fig. 8. It was shown that the birefringence pattern was quite similar to the image of the residual stress presented in Fig. 7. This indicates that this numerical simulation accounts for the ICM process successfully.

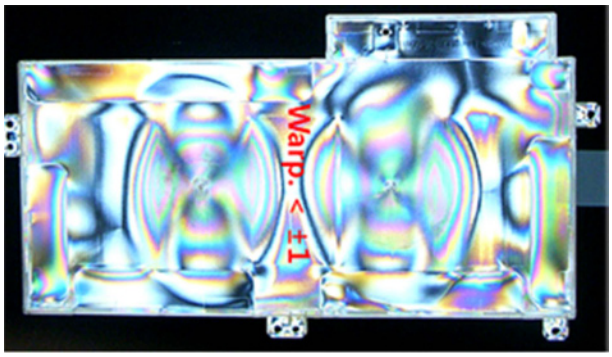

Fig. 8. (Color online) Birefringence image of the molded part.

4. Conclusions

We exploited the ICM process in order to manufacture thin-walled polymeric parts. A battery case was designed and injection-molded experimentally. The molding process was numerically simulated to understand flow and heat transfer behavior in the mold cavity. The resulting filling pressure, clamping force, filling time, pressure, residual stress, and warpage were analyzed. In addition, birefringence of the molded part was measured and compared with the result of the residual stress obtained numerically. We expect that this study provides meaningful insight into ICM for wider applications of the process.

References

Chen, H.L., S.C. Chen, W.H. Liao, R.D. Chien, and Y.T. Lin, 2013, Effects of insert film on asymmetric mold temperature and associated part warpage during in-mold decoration injection molding of PP parts, *Int. Commun. Heat Mass Transf.* **41**, 34-40.

Chen, S.C., Y.C. Chen, N.T. Cheng, and M.S. Huang, 1998, Simulation of injection-compression mold-filling process, *Int. Commun. Heat Mass Transf.* **25**, 907-917.

Guevara-Morales, A. and U. Figueroa-López, 2014, Residual stresses in injection molded products, *J. Mater. Sci.* **49**, 4399-4415.

Hong, S., J. Hwang, J. Kang, and K. Yoon, 2015, Comparison of injection molding and injection/compression molding for the replication of microstructure, *Korea-Aust. Rheol. J.* **27**, 309-317.

Isayev, A.I., G.D. Shyu, and C.T. Li, 2006, Residual stresses and birefringence in injection molding of amorphous polymers: Simulation and comparison with experiment, *J. Polym. Sci. Pt. B-Polym. Phys.* **44**, 622-639.

Jiang, H., G.T. Lim, J.N. Reddy, J.D. Whitcomb, and H.J. Sue, 2007, Finite element method parametric study on scratch behavior of polymers, *J. Polym. Sci. Pt. B-Polym. Phys.* **45**, 1435-1447.

Kabanemi, K.K., H. Vaillancourt, H. Wang, and G. Salloum, 1998, Residual stresses, shrinkage, and warpage of complex injection molded products: Numerical simulation and experimental validation, *Polym. Eng. Sci.* **38**, 21-37.

Kamal, M.R., R.A. Lai-Fook, and J.R. Hernandez-Aguilar, 2002, Residual thermal stresses in injection moldings of thermoplastics: A theoretical and experimental study, *Polym. Eng. Sci.* **42**, 1098-1114.

Min, I. and K. Yoon, 2011, An experimental study on the effects of injection-molding types for the birefringence distribution in polycarbonate discs, *Korea-Aust. Rheol. J.* **23**, 155-162.

Oh, H.J. and Y.S. Song, 2015, Precise nanoinjection molding through local film heating system, *RSC Adv.* **5**, 99797-99805.

Oh, H.J. and Y.S. Song, 2017, Surface strengthening of injection molded parts by applying a thermal insulation film, *RSC Adv.* **7**, 14302-14308.

Oh, H.J., Y.S. Song, S.H. Kim, S.Y. Kim, and J.R. Youn, 2011, Fluid-structure interaction analysis on the film wrinkling problem of a film insert molded part, *Polym. Eng. Sci.* **51**, 812-818.

Ozcelik, B. and I. Sonat, 2009, Warpage and structural analysis of thin shell plastic in the plastic injection molding, *Mater. Des.* **30**, 367-375.

Teixeira, D., M. Giovanela, L.B. Gonella, and J.S. Crespo, 2015, Influence of injection molding on the flexural strength and surface quality of long glass fiber-reinforced polyamide 6.6 composites, *Mater. Des.* **85**, 695-706.

Weng, C., W.B. Lee, and S. To, 2009a, Birefringence techniques for the characterization of residual stresses in injection-moulded micro-lens arrays, *Polym. Test* **28**, 709-714.

Weng, C., W.B. Lee, S. To, and B.Y. Jiang, 2009b, Numerical simulation of residual stress and birefringence in the precision injection molding of plastic microlens arrays, *Int. Commun. Heat Mass Transf.* **36**, 213-219.